On the Nature and Origin of Si Surface Segregation in Amorphous AuSi Alloys

Soo-Hwan Lee, J. Adam Stephens, and Gyeong S. Hwang*

Department of Chemical Engineering, The University of Texas at Austin, Austin, Texas 78713

Received: October 10, 2009; Revised Manuscript Received: January 9, 2010

We examined the surface segregation behavior of Si in amorphous AuSi alloys using ab initio molecular dynamics simulations within density functional theory. For a thin $Au_{70}Si_{30}$ film, our simulations predict Si surface enrichment that leads to a stoichiometry close to $Au_{60}Si_{40}$ in the surface layer. The surface structure exhibits a rather ordered Au_3Si_2 phase, which somewhat differs from the bulk $Au_{60}Si_{40}$ structure that exhibits a tendency of random hard-sphere packing. We also discuss the origin of the Si surface segregation based on analysis of segregation-induced changes in the atomic and electronic structure of the AuSi alloy surface.

Introduction

Surface segregation in a binary alloy refers to the phenomenon by which one component of the alloy is enriched near the surface, relative to its bulk composition. The surface composition change can alter the surface characteristics of alloy materials and, thus, plays an important role in many relevant surface-related applications such as catalysis, tribology, oxidation, and growth. Therefore, the nature and causes of surface segregation have long been an important subject of study. The segregation behavior arises because of the disparity in the local atomic environment between surface and bulk regions. From a thermodynamic point of view, it can be explained by Gibbs free energy minimization through exchange of surface and bulk atoms. Earlier phenomenological studies[1−3] highlighted the importance of heat of solution, surface energies, and atomic size differences in establishing surface segregation tendencies. However, atomistic details of the segregation, structure and mechanism remain ambiguous for many alloy systems.

Gold (Au) has been found to be very reactive toward silicon (Si), although it is well-known to be a very stable and nonreactive noble metal. It has been observed that Au deposition on a Si substrate leads to silicide formation even at room temperature;[4] in particular, Si substrate atoms tend to diffuse out through an Au overlayer and form an AuSi alloy at the top Au layer.[5] There have been substantial efforts[4−10] to elucidate the surface phase and electronic structure of AuSi alloys, yet uncertainty remains. Recently, Hoshino and co-workers[6] reported Au_3Si_2 phase formation at the top layer of Au deposited on Si(111) at room temperature when the Au coverage is above 5.2 monolayers (MLs), based on high resolution medium energy ion scattering (MEIS) combined with photoelectron spectroscopy (PES). Using X-ray measurements, Shpyrko and co-workers[8] presented evidence for surface crystallization and enhanced surface layering in the liquid $Au_{82}Si_{18}$ alloy. While direct experimental evidence is lacking, to our knowledge no detailed theoretical study has been reported on the nature and origin of the surface segregation of amorphous AuSi alloys.

In this paper, we use density functional theory based ab initio molecular dynamics (AIMD) to determine the surface structure of an AuSi amorphous alloy. We also discuss the origin of Si surface segregation based on theoretical analysis of segregation-induced changes in the surface atomic and electronic structures. For a model system, we choose a thin amorphous $Au_{70}Si_{30}$ film. Besides its scientific significance as a prototype for understanding the nature of metallic alloy surfaces, the AuSi system has recently received great attention because of its technological importance, such as Au catalyzed growth of Si nanowires.[11,12] In particular, the fundamental findings from this theoretical work can provide some insight into how Si atoms will be dissolved in an Au nanoparticle and how they will be supplied to the interface between the Au particle and the growing Si nanowire. Moreover, the results of the present study can complement existing experimental observations and also clarify microscopic mechanisms underlying Au−Si alloying in the fabrication and operation of various relevant devices.

Computational Details

AIMD and static structural optimization were performed using the well-established planewave program VASP (Vienna Ab initio simulation package).[13] We used the generalized gradient approximation (GGA) derived by Perdew and Wang (PW91)[14] to density functional theory (DFT). Vanderbilt-type ultrasoft pseudopotentials[15] were employed to describe the ion−electron interaction with valence configurations of $5d^{10}\ 6s^1$ for Au and $3s^2\ 3p^2$ for Si. Outer electron wave functions were expanded using a plane-wave basis set with a kinetic energy cutoff of 270 eV. The Brillouin zone integration was performed using one k-point (at Gamma). All atoms were fully relaxed using the conjugate gradient method until residual forces on constituent atoms became smaller than 5×10^{-2} eV/Å.

For a model system, we prepared a roughly 16 Å-thick slab of amorphous $Au_{70}Si_{30}$ with 134 Au and 58 Si atoms. The initial slab structure was created by inserting a vacuum layer into the $Au_{70}Si_{30}$ bulk that was generated using combined modified embedded atom method (MEAM) and AIMD simulations,[16] followed by AIMD annealing for surface structure relaxation. Therefore, Au and Si atoms initially were distributed almost uniformly throughout the slab. Note that the constituent Au and Si atoms in an amorphous Au−Si bulk alloy are predicted to be well mixed with no segregation.[16]

To examine how the presence of flat surfaces affects the atomic distribution within the slab, we performed a series of AIMD simulations in the canonical ensemble with varying temperatures [see Figure 1]. All atoms were allowed to move at 800 K and subsequently 600 K for about 2 ps each, followed

* To whom correspondence should be addressed. E-mail: gshwang@che.utexas.edu. Phone: 512-471-4847. Fax: 512-471-7060.

10.1021/jp9097099
Published on Web 02/03/2010

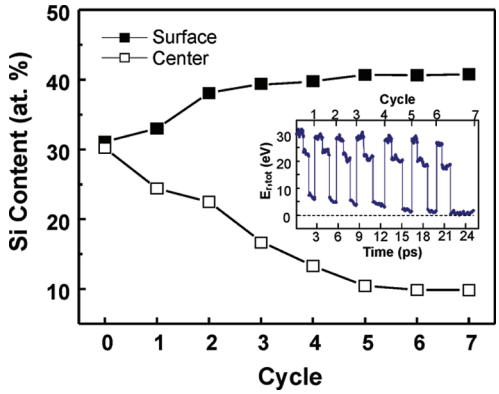

Figure 1. (Color online) Variation in the Si content at the surface and center layers of the AuSi slab (sketched in Figure 2) as a function of annealing cycle. The inset shows a variation in the relative total energy ($E_{r,tot}$) of the AuSi slab during the AIMD simulation; the corresponding annealing time is also indicated.

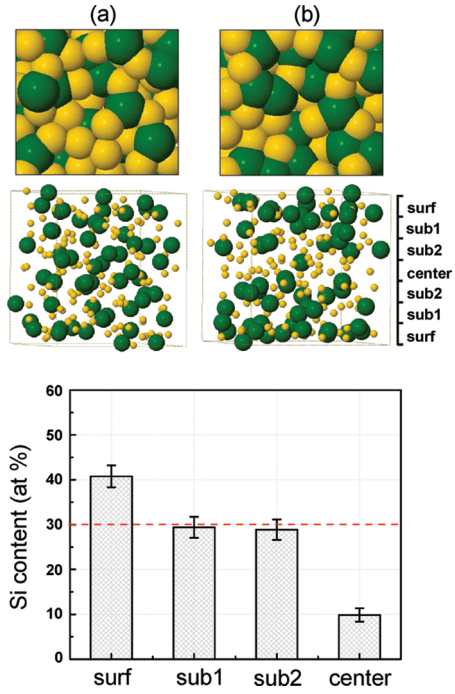

Figure 2. Top (top panels) and side (middle panels) views of the thin $Au_{70}Si_{30}$ slab (a) before and (b) after Si surface segregation. The bottom panel shows Si contents in the surface, subsurface, and center layers (as indicated), obtained during 4 ps AIMD at 300 K in the seventh cycle. Initially, 134 Au and 58 Si atoms were almost uniformly distributed in the 16 Å thick AuSi slab, as shown in (a). The dark green (black) and yellow (gray) balls represent Si and Au atoms, respectively.

by relaxation at 300 K for about 2 ps (except the seventh cycle where the relaxation at 300 K was performed for 4 ps). The annealing steps were repeated until the AuSi system reached steady state. As illustrated in Figure 1, seven cycles of the annealing procedure are likely sufficient to obtain the steady state distribution of Au and Si atoms in the direction perpendicular to the slab.

Results and Discussions

Si Surface Segregation. Figure 2 shows the variation in the Si content along the direction perpendicular to the slab, which was obtained during 4 ps AIMD at 300 K in the seventh cycle. Here the composition ratio plot was obtained by averaging the upper and lower layers of the slab (as illustrated in the right middle panel of Figure 2). Although thermal fluctuations in the atomic distribution are noticeable, the results explicitly demonstrate that Si atoms are enriched in the surface layer while significantly depleted in the center layer. Beginning from a uniformly mixed slab with an overall Si composition of 30 at. %, the steady state distribution exhibits Si enrichment in the surface layer to 40 at. % and Si depletion in the center layer to less than 10 at. %. The top- and side-view snapshots before and after the atomic rearrangements also clearly demonstrate the surface enrichment of Si atoms. In the first and second subsurface layers, the Au−Si alloy has a stoichiometry (on average) close to $Au_{70}Si_{30}$.

Another interesting feature from our calculation results is that the surface layer has a higher atomic density than the subsurface layers; the surface/subsurface atomic ratio is predicted to be ≈1.3. The increased density of surface atoms as a result of the Si surface enrichment tends to result in enhancement of surface bonds and consequent stabilization of the alloy surface (as demonstrated by the surface electronic structure analysis later). This is consistent with earlier X-ray reflectivity measurements that demonstrated the presence of high-density surface layers in liquid metals.[17]

Here it is worth emphasizing that the Si content drastically reduces below 10 at. % in the center layer while the top three layers contain 30−40 at. % Si, leading to a rather box-like Si concentration profile near the surface. The result may suggest the formation and gradual growth of an AuSi alloy layer (with 30−40 at. % of Si) from the surface when Si atoms are introduced to an Au film or particle. This finding could be supported by recent XPS measurements that showed a large enrichment of Si at the top few atomic layers of the $Au_{82}Si_{18}$ alloy.[9] This is also consistent with recent theoretical predictions[16] that (i) the bulk AuSi amorphous alloy may form the most stable structure when the Si content is around 40−50 at. % and (ii) the mixing enthalpy becomes slightly positive when the Si content is small (<10 at. %), implying the possible existence of a barrier for incorporation of Si atoms into an Au layer with such low Si content [see Figure 1a in ref 16]. These findings may also suggest (in association with Au-catalyzed Si nanowire growth) that: i) Si atoms would be incorporated into an Au catalyst particle mostly by forming an AuSi alloy near the surface if the Au particle is sufficiently large, and ii) the dissolved Si atoms would undergo diffusion along the near-surface alloy region and precipitate at the interface between the Au catalyst and the growing Si nanowire. More details on the vapor−liquid−solid growth mechanism of Si nanowires will be presented elsewhere.

Surface Atomic Structure. To analyze the surface atomic structure of the $Au_{70}Si_{30}$ alloy slab, we calculated the planar radial distribution function [PRDF, g(r)] which is the ratio of the local atomic density to the overall atomic density. It is averaged over all the atoms in the surface and plotted as a function of distance from atomic center. Here, the planar variant of the RDF is determined by

$$g(r) = \left\langle \frac{Ah(r, r + \Delta r)}{n^2 2\pi r \Delta r} \right\rangle$$

where A and n are the area of and number of atoms contained in the surface layer, respectively, and Δr is the histogram bin width. The histogram $h(r, r + \Delta r)$ is constructed by iterating over the surface atoms and binning the neighbors of each according to the component of their separation which is parallel

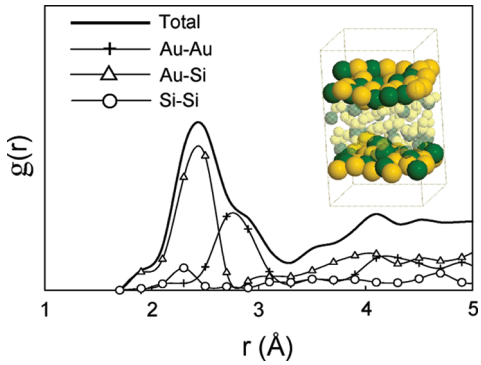

Figure 3. Planar radial distribution function [PRDF, $g(r)$] for the surface of the $Au_{70}Si_{30}$ alloy slab. The PDRF was obtained by averaging over the top and bottom surfaces (as indicated in the inset) of five independent frames taken from the 7th annealing cycle (300 K) of the AIMD simulation and relaxed by static geometry optimization. The dark green (black) and yellow (gray) balls in the inset represent Si and Au atoms, respectively.

to the surface plane. The angle brackets denote an ensemble average. The surface of our amorphous slab was not well-defined, so we chose to include in our PRDF calculation only those atoms whose surface-projected coordinates had no overlap with those of other atoms nearer the surface, as illustrated in the inset of Figure 3. The overlap radius (=1.9 Å) was based on the projection of a bond of typical length (the approximate average of the Au−Au and Si−Si equilibrium separations) making a 45° angle with the surface plane. The component plots (Au−Au, Au−Si, and Si−Si) were generated by recording separate histograms for each pair of elements, then normalizing using the total areal density.

The PRDF [$g(r)$] in Figure 3 was obtained by averaging over the top and bottom surfaces of five independent frames which were taken from the seventh annealing cycle (300K) of the AIMD simulation and relaxed by static geometry optimization. The total PRDF has a distinct peak at around 2.4 Å due almost entirely to the Au−Si component and a shoulder at around 2.8 Å caused by a peak in the Au−Au component. The first peak in the Si−Si component at about 2.3 Å makes a relatively small contribution to the total PRDF. The first minimum in the PRDF occurs at 3.3 Å, after which there are fewer well-defined features. These features clearly show that the first neighbor shells of surface Si atoms are occupied mostly by Au atoms, while Au atoms are surrounded by a more balanced mixture of Au and Si neighbors.

By taking the first minimum in the PRDF as the nearest neighbor cutoff radius, we attempted to determine the coordination numbers of all the surface atoms in the aforementioned five independent frames. For the cutoff radius of 3.3 Å we found that each Si atom is surrounded by an average of 3.5 Au and 1.2 Si atoms while each Au atom has 2.7 Au and 2.5 Si neighbors, which corresponds to an Au/Si ratio of ≈1.5. The calculation result is well supported by previous experiments that demonstrated Au-rich silicide formation with an Au/Si ratio of 1.5 based on low energy scattering analysis[7] and electron-induced Auger electron spectroscopy.[4] The $Au_{60}Si_{40}$ structure is also consistent with a recent experimental study that reported $Au_{60}Si_{40}$ phase formation at the surface of a sufficiently thick (≈5.2−12.8 MLs) Au layer grown on Si(111) at room temperature.[6]

Compared to the surface alloy, the atomic structure of bulk $Au_{60}Si_{40}$ looks somewhat different. In contrast to the rather ordered Au_3Si_2 phase (in which Si and Au atoms tend to prefer

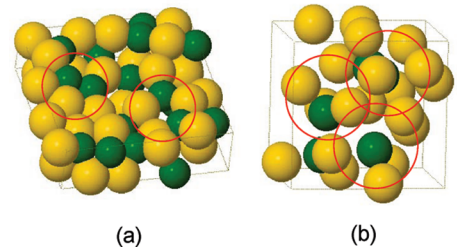

Figure 4. Atomic structures of the $Au_{60}Si_{40}$ alloy: (a) near surface and (b) in bulk, taken from AIMD snapshots with structure optimization. The dark green (black) and yellow (gray) balls represent Si and Au atoms, respectively.

to be surrounded by dissimilar atoms with a higher coordination number [see Figure 4a]), the bulk structure in Figure 4b exhibits a tendency of random hard-sphere packing (as often seen in amorphous metal alloys) with no segregation on the whole.[16] The difference between the surface and bulk alloys in nature could also explain the possible occurrence of surface-induced atomic layering in AuSi alloys as suggested by recent X-ray measurements,[8] although the exact near-surface structure may vary with stoichiometry and/or other factors.

Surface Electronic Structure. Next we examined how the Si surface segregation affects the surface electronic structure of the AuSi alloy. A recent theoretical study[16] showed occurrence of strong hybridization of Au 5d states with Si 3p states, which appears to be mainly responsible for AuSi alloy stabilization. In addition, earlier experiments[18] evidenced a significant change in the Au 5d feature upon Au−Si alloy formation when Au was deposited on Si or vice versa. To understand the possible correlation of the electronic structure change and the Si surface segregation, we calculated changes in the partial density of states (PDOS) of Au and Si atoms with varying Si/Au distributions across the slab thickness.

Figure 5 shows the 5d PDOS of Au in the near-surface and center regions of the AuSi alloy slab, together with corresponding features in pure crystalline Au for comparison. Here, the Fermi level is used as the reference energy state (which is set to be zero). The most important feature from the results is that the surface states 1.5−3 eV below the Fermi level, which are strongly pronounced at the pure Au surface due to d−d antibonding, gradually vanish as Si atoms are enriched at the surface. This is consistent with previous photoemission experiments which demonstrated attenuation in the antibonding d−d state features when the AuSi alloy layer was formed on pure Au.[18] Another important feature is that in the near-surface region the Au 5d states (particularly 2−3 eV below the Fermi level) are noticeably reduced as the Si content is increased from 30 to 40 at. %, but the corresponding states in the center region remain practically unchanged with the reduction of Si content. The shift of the surface 5d state to a higher binding energy indicates that the surface structure is better stabilized, thereby lowering the total energy. On the other hand, the depletion of Si atoms in the center region may reduce the hybridization strength between the Au 5d and Si 3p states, but this effect is likely to be insignificant according to our calculations. In fact, our recent DFT study[16] predicted that in the bulk Au−Si alloy the enthalpy of mixing varies insignificantly as Si content is lowered from 30 to 10 at. %.

Figure 6 presents the Au 5d and Si 3d PDOS for surface and bulk $Au_{60}Si_{40}$ alloys, both exhibiting a significant shift in the Si 3p and Au 5d states to higher binding energies compared to their pure counterparts[16] with a high degree of p−d hybridization in the energy range between −4 and −7 eV. This unambigu-

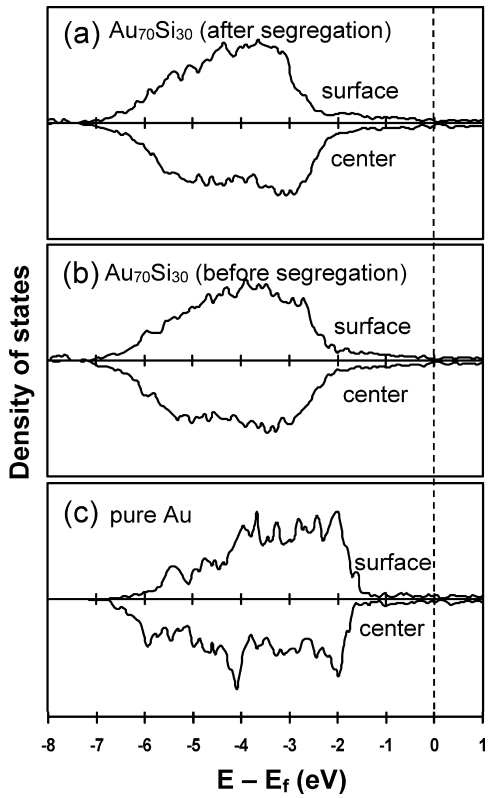

Figure 5. Density of states (DOS) of the surface and center layers of the $Au_{70}Si_{30}$ slab structure, as indicated in Figure 1, (a) after and (b) before Si surface segregation, together with (c) those of the pure Au slab structure for the sake of comparison. The dotted line indicates the Fermi level position.

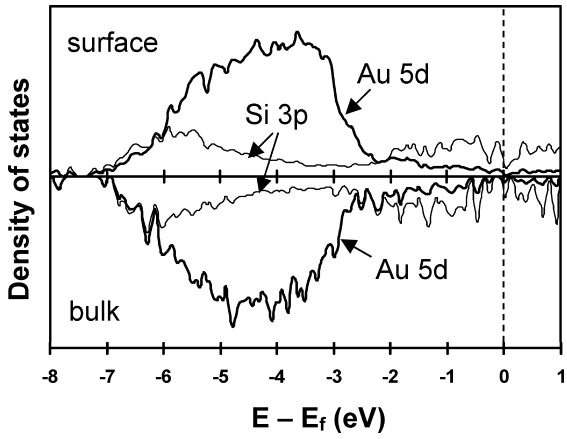

Figure 6. Local density of states (LDOS) projected on Au and Si atoms in the $Au_{60}Si_{40}$ structure: (a) near surface and (b) in bulk. The dotted line indicates the Fermi level position.

ously illustrates the importance of p−d hybridization in stabilizing both surface and bulk alloys. In addition, no gap at the Fermi level is seen in the computed DOS profiles, indicating the Au−Si alloys are metallic.

Finally we calculated the work function of the AuSi alloy surface. The work function (WF) is by definition the minimum energy required to remove an electron to a position far from the surface. Using the DFT method, the WF in slab geometry can be evaluated reasonably well by $WF = V(\infty) - E_F$, where $V(\infty)$ and E_F represent the electronic potential in a vacuum region far from the surface and the Fermi energy of the neutral surface system, respectively. For a well relaxed surface of the AuSi alloy slab, our DFT-GGA calculations predicted the WF to be about 4.9 eV. This value is close to 4.86 ± 0.05[19] and 4.97 ± 0.02 eV[20] as previously measured for PtSi, while PtSi and AuSi alloy surfaces are expected to have a comparable work function. For comparison purpose, we also computed the work function of pure Au(111); the predicted value of 5.27 eV is in good agreement with experimental values of 5.20[21] and 5.35 eV.[22]

Conclusions

We have performed ab initio molecular dynamics (AIMD) and static structural optimization within the framework of the gradient corrected density functional theory to identify the surface segregation, structure, and electron density of states of an AuSi amorphous alloy. For a thin $Au_{70}Si_{30}$ layer which initially has a uniform Si distribution at 30 at. %, our AIMD results clearly show the occurrence of Si surface segregation that results in a stoichiometry close to $Au_{60}Si_{40}$ near the surface, while the Si content is maintained at about 30 at. % in the first and second subsurface layers and below 10 at. % in the third subsurface (center) layer. Our calculations also demonstrate that the surface layer has a higher atomic density than the subsurface layers, as also often seen in liquid metals. The alloying-induced increase in the surface atomic density leads to enhancement of surface bonds and consequent stabilization of the AuSi alloy surface. We also find that the Si content drastically reduces below 10 at. % in the center layer while the top three layers contain 30−40 at. % Si, rather than a gradual change in the Si concentration profile. The box-like profile may suggest the formation and gradual growth of an AuSi alloy layer from the surface, if Si atoms are continuously supplied to an Au film or particle. The surface atomic structure of the AuSi alloy slab was analyzed using the planar radial distribution function. The surface layer structure exhibits a rather ordered Au_3Si_2 phase in which Si and Au atoms tend to prefer to be surrounded by dissimilar atoms with a higher coordination number, which is somewhat different from the AuSi bulk structure that shows a tendency of random hard-sphere packing as often seen in amorphous metal alloys. We also calculated the Si segregation-induced changes of surface electronic structure. The results show that the surface states 1.5−3 eV below the Fermi level gradually vanish as Si atoms are segregated near the surface, while they are strongly pronounced at the pure Au surface due to d−d antibonding. The electronic structure analysis also highlights the importance of hybridization of Au 5d states with Si 3p states in determining the structure of both surface and bulk alloys. Finally, our calculations predicted the AuSi work function to be 4.9 eV, which is close to previously measured values for the PtSi alloy surface.

Acknowledgment. We acknowledge the Robert A. Welch Foundation (F-1535) for the support of this work. All of our calculations were performed using supercomputers in Texas Advanced Computing Center at the University of Texas at Austin.

References and Notes

(1) Hamilton, J. C. *Phys. Rev. Lett.* **1979**, *42*, 989.
(2) Williams, F. L.; Nason, D. *Surf. Sci.* **1974**, *45*, 377.
(3) Lin, Z.; Xu, F.; Weaver, J. H. *Phys. Rev. B* **1987**, *36*, 5777.
(4) Kim, J. H.; Yang, G.; Yang, S.; Weiss, A. H. *Surf. Sci.* **2001**, *475*, 37.
(5) Hiraki, A.; Lugujjo, E.; Mayer, J. W. *J. Appl. Phys.* **1972**, *43*, 3643.
(6) Hoshino, Y.; Kitsudo, Y.; Iwami, M.; Kido, Y. *Surf. Sci.* **2008**, *602*, 2089.
(7) Ceelen, W. C. A. N.; Moest, B.; Ridder, M.; van Ijzendoorn, L. J.; van der Gon, A. W. D.; Brongersma, H. H. *Appl. Surf. Sci.* **1998**, *134*, 87.

(8) Shpyrko, O. G.; Streitel, R.; Balagurusamy, V. S. K.; Grigoriev, A. Y.; Deutsch, M.; Ocko, B. M.; Meron, M.; Lin, B.; Pershan, P. S. *Science* **2006**, *313*, 77.

(9) Halka, V.; Streitel, R.; Freyland, W. *J. Phys.: Condens. Matter* **2008**, *20*, 355007.

(10) Kuo, C. L.; Clancy, P. *Surf. Sci.* **2004**, *551*, 39.

(11) Hannon, J. B.; Kodambaka, S.; Ross, F. M.; Tromp, R. M. *Nature* **2006**, *440*, 69.

(12) Wu, Y.; Yang, P. *J. Am. Chem. Soc.* **2001**, *123*, 3165.

(13) Kresse, G.; Furthmuller, J. *VASP the guide*; Vienna University of Technology: Vienna, 2001.

(14) Perdew, J.; Chevary, J.; Vosko, S.; Jackson, K.; Pederson, M.; Singh, D.; Fiolhais, C. *Phys. Rev. B* **1992**, *46*, 6671.

(15) Vanderbilt, D. *Phys. Rev. B* **1990**, *41*, 7892.

(16) Lee, S. H.; Hwang, G. S. *J. Chem. Phys.* **2007**, *127*, 224710.

(17) Shpyrko, O. G.; Grigoriev, A. Y.; Steimer, C.; Pershan, P. S.; Lin, B.; Meron, M.; Graber, T.; Gerbhardt, J.; Ocko, B.; Deutsch, M. *Phys. Rev. B* **2004**, *70*, 224206.

(18) Franciosi, A.; Niles, D. W.; Margaritondo, G.; Quaresima, C.; Capozi, M.; Perfetti, P. *Phys. Rev. B* **1985**, *32*, 6917.

(19) Bucher, E.; Schulz, S.; Ch, M.; Munz, P.; Gubler, U.; Greuter, F. *Appl. Phys. A: Mater. Sci. Process.* **1986**, *40*, 71.

(20) Freeouf, J. L. *Solid State Commun.* **1980**, *33*, 1059.

(21) Heimel, G.; Romaner, L.; Bredas, J.-L.; Zojer, E. *Phys. Rev. Lett.* **2006**, *96*, 196806.

(22) De Renzi, V.; Rousseau, R.; Marchetto, D.; Biagi, R.; Scandolo, S.; del Pennino, U. *Phys. Rev. Lett.* **2005**, *95*, 046804.

JP9097099